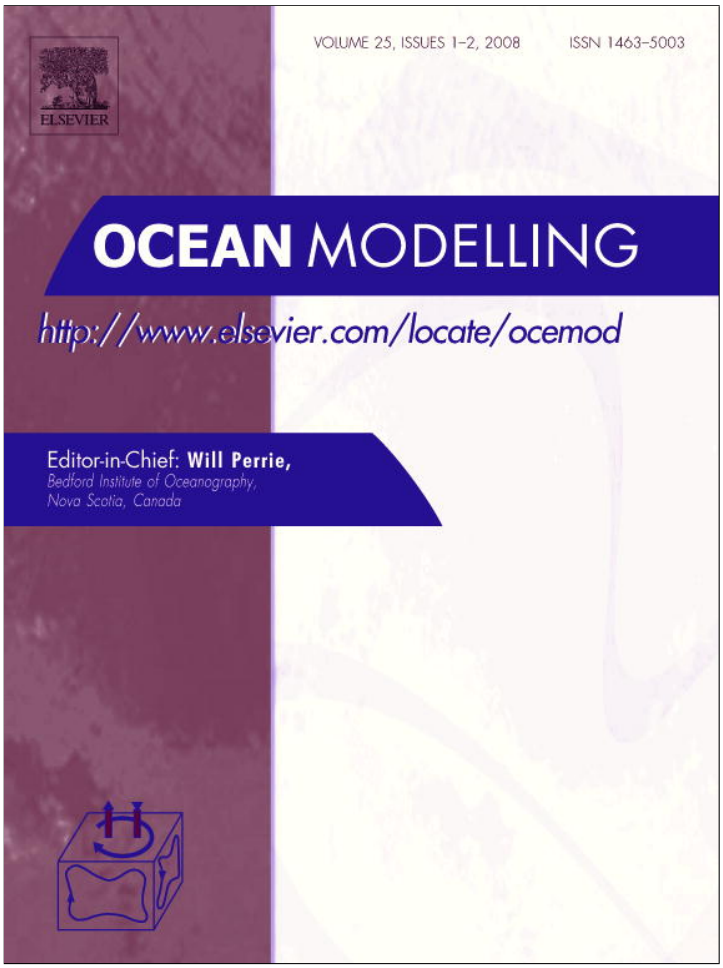

Ocean Modelling 25 (2008) 35–47

Contents lists available at ScienceDirect

Ocean Modelling

journal homepage: www.elsevier.com/locate/ocemod

A mosaic approach to wind wave modeling ☆

Hendrik L. Tolman *

NOAA/NCEP/EMC Marine Modeling and Analysis Branch, 5200 Auth Road Room 209, Camp Springs, MD 20746, USA

ARTICLE INFO

Article history:
Received 18 February 2008
Received in revised form 30 April 2008
Accepted 10 June 2008
Available online 26 June 2008

Keywords:
Wind waves
Numerical methods
Mosaic grid approach

ABSTRACT

A mosaic or multi-grid approach to wind wave modeling is presented. In this approach, a series of grids with different resolutions are treated as individual wave models, while simultaneously and continuously considering interactions between these grids. This converts a mosaic of grids into a single wave model. For overlapping grids with distinctly different resolutions, two-way nesting is introduced. For overlapping grids with similar resolution, a reconciliation method is introduced. These techniques are implemented in the WAVEWATCH III wind wave model and are tested for several idealized situations, and for a realistic wave hindcast for coastal Alaskan waters. The mosaic approach is shown to give consistent results across grid scales and provides an effective and economical way to locally increase the spatial resolution of wave models.

Published by Elsevier Ltd.

1. Introduction

Numerical wind wave modeling has been practiced since the mid 1950's for a variety of purposes, such as operational forecasting, coastal engineering design and coastal evolution studies, and general wind wave research. Traditionally, wind wave modeling has been most actively pursued by coastal engineers. A large majority of present wind wave models and wave model applications use a Eulerian structured grid approach with typically Cartesian or spherical (longitude–latitude) grids.

The main focus of wave studies is often on wave conditions in coastal areas. Traditionally, such conditions are modeled with a local high-resolution wave model, which gets its boundary conditions from lower resolution models covering larger areas. If necessary a set of telescoping grids is considered. None of the presently available wind wave models provides information from high resolution grids back to lower resolution grids. Hence, nesting in traditional wind wave models is characterized as one-way nesting.

The one-way nesting approach has drawbacks, in particular for hurricane wave modeling, where the dominant wind waves are generated near the core of the hurricane. Accurate modeling of such waves requires high resolution. When these wind waves become swell while traveling away from the hurricane, spatial and temporal scales of the wave field increase. Such waves can be modeled accurately at lower resolution, if the low resolution model obtains data from a higher resolution model near the core of the hurricane. The latter data flow is traditionally not provided in one-way nested wave models. Note that high resolution grids near the core of the hurricane should ideally be relocatable, as is common practice in hurricane (weather) modeling (e.g. Kurihara et al., 1995).

Other drawbacks of a one-way nesting approach can be found in typical modeling requirements at operational forecast centers, such as the National Centers for Environmental Prediction (NCEP). At NCEP, wave model guidance needs to be produced at three distinct scales; deep ocean, offshore and coastal. One way nesting approaches are not conducive to providing consistent model guidance at such a range of scales. In a more general sense, one-way nesting does not produce seamless modeling of wind waves from the deep ocean to the surf zone.

Conventional one-way nesting is performed to focus model resolution in desired areas. More advanced methods of achieving this have been introduced. Gomez and Carretero (1997) have presented a version of the WAM model (Komen et al., 1994) featuring a stepwise increased resolution in an otherwise conventional structured grid. The systematic layout of areas with specific grid resolutions suggests that this can loosely be interpreted as two-way nesting. Alternately, curvilinear grids can be used to focus resolution in areas of interest. This approach is available in recent versions of the SWAN model (Booij et al., 1999; Ris et al., 1999). Unstructured spatial grids are explicitly designed to focus resolution in areas of interest. Early wave models use semi-Lagrangian characteristics methods on unstructured grids (Benoit et al., 1996; Ardhuin et al., 2001). More recently, Eulerian finite element methods have been introduced in wave models (Hsu et al., 2005). Note that in the latter approaches only the spatial grid becomes unstructured. Spectral grids remain structured, particularly to facilitate computation of nonlinear wave-wave interactions.

The present study explores the development of a two-way nested approach to wave modeling as an alternative to target areas

☆ MMAB contribution Nr. 267.

* Tel.: +1 301 763 8000x7253; fax: +1 301 763 8545.
E-mail address: hendrik.tolman@noaa.gov

1463-5003/$ - see front matter Published by Elsevier Ltd.
doi:10.1016/j.ocemod.2008.06.005

for high resolution wave modeling. In this approach, the area to be modeled is covered with a mosaic of grids with arbitrary resolution. Each grid will be considered as a separate wave model. Two-way interaction between all grids will be considered continuously, transforming the mosaic of individual grids into a single model. This approach can be considered as a generalization of the approach of Gomez and Carretero (1997). In the present manuscript, only static grids will be considered. The approach is tested in the WAVEWATCH III wave model (Tolman, 1991; Tolman, 2002; Tolman et al., 2002), and was implemented operationally at NCEP in November 2007 (Chawla et al., 2007).

The basic concepts and assumptions of this two-way nesting approach are discussed in Section 2, including necessary adaptations to the WAVEWATCH III model. Section 3 deals with the details and the testing of the nesting techniques. A special case occurs when grids with similar resolutions overlap, which is discussed in Section 4. A practical application to Alaskan waters and island blocking by the Aleutian islands is presented in Section 5. Discussion and conclusions are presented in Sections 6 and 7.

2. Basic approaches

The present study develops a mosaic approach to wind wave modeling where an arbitrary number of grids, with arbitrary resolutions, are considered with full two-way interaction between all grids. At the center of the mosaic approach, the solution for each grid is propagated for a single time step as in a conventional wave model. The solution is propagated in time by solving the spectral action balance equation

$$\frac{\partial N}{\partial t} + \nabla_x \cdot \boldsymbol{c}_x N + \nabla_s \cdot \boldsymbol{c}_s N = S, \tag{1}$$

where N is the spectral action density, ∇_x, ∇_s, $\boldsymbol{c}_x$ and $\boldsymbol{c}_s$ are the divergence and characteristic velocities in physical and spectral space, respectively, and S represents all source terms describing wave growth, attenuation and nonlinear wave-wave interactions. The spectral space is defined by the intrinsic frequency σ, the wave number k, and the spectral direction θ (or wavenumber vector $\boldsymbol{k}$). These are interrelated in the dispersion relation

$$\sigma^2 = gk \tanh kd, \tag{2}$$

where d is the mean water depth. Hence, spectral space is defined by two independent parameters. In WAVEWATCH III (henceforth denoted as WW3), the spectral space is defined as (k,θ). In WW3, Eq. (1) is solved using a fractional step method (Yanenko, 1971), where spatial propagation (second term on left side), intra-spectral propagation (third term on left side) and source terms (right side of equation) are considered consecutively. The action density spectrum $N(k,\theta) \equiv F(k,\theta)/\sigma$, where F is the conventional energy density spectrum.

Considering grids as separate wave models inside the mosaic approach implies consecutive computation of individual grids. The appropriate data transfer depends on the relative resolution between grids. Providing boundary data from lower resolution grids to higher resolution grids is a long established method of one-way nesting in WW3 and other wave models. This implies that wave conditions in lower resolution grids need to be computed before higher resolution grids can be considered. A natural way of converting information back from high resolution grids to lower resolution grids is to replace grid point spectra in the lower resolution grid with the average spectral values of that part of the higher resolution grid that covers the corresponding low resolution grid cell. This can only be done once the computation for the high resolution grid has caught up with the low resolution grid. Details of this two-way nesting approach and tests are presented in Section 3.

A special case occurs when grids with comparable resolutions overlap. This may be beneficial for breaking up long and narrow shelf regions into manageable individual grids, or for stepwise reduction of longitudinal resolution with latitude. The latter maintains comparable physical resolutions and time steps with increasing latitudes in spherical grids. For overlapping grids with similar resolution, no clear computational order between grids can be established. Hence, solutions for each grid will be considered individually, after which the solutions in the overlap areas of the grids are reconciled. Details of this approach and corresponding tests are presented in Section 4.

With the introduction of the overlapping grids with similar but not identical resolutions, the user of the model needs to identify which grids are considered to be overlapping, and which grids are considered to be nested. To make this possible, a grid rank is introduced (by the user), where the lowest rank corresponds to the lowest resolution. A model can only check if assigned ranks are consistent with provided grid resolutions.

With the above basic techniques for two-way nesting and overlapping grids, several necessary steps need to be taken for each grid individually and sequentially, as outlined in Table 1. These steps are repeated until all requested model integration and output have been completed. Note that all these steps are generic for the approach, and are not dictated by the choice of the WW3 model. In many of these steps, there is communication among grids in the mosaic approach. However, only step 3 needs to consider several grids simultaneously. Availability of boundary data, maximum time steps for each grid and times for output requests determine the next synchronization time.

The nine steps of Table 1 provide a sufficient set of logical requirements to develop a generally applicable grid management algorithm. However, to simplify its implementation, additional consideration are introduced:

(1) The nine steps in Table 1 enforce local synchronization between grids only. The algorithm is greatly simplified if a global synchronization time is adopted. Naturally, this would be the synchronization time of the lowest ranked grids. Note that this does not necessarily require that time steps for different ranked grids are integer multiples.
(2) For groups of grids with identical rank synchronization times are kept identical, in order to better control load balancing for distributed computing.
(3) To simplify the determination of relations between grids, grid points where boundary data from lower ranked grids are expected are explicitly defined by the user. Unlike the previous two requirements, this requirement is specifically adopted for implementation in WW3.

Table 1
Necessary sequential steps to be taken for each individual grid, defining the multi-grid management algorithm (repeated until model integration and output are completed)

Step	Action
1.	Update input fields for the grid as needed
2.	Update boundary data from lower resolution grids
3.	Update the model time step and the next synchronization time for the relevant grids
4.	Run the wave model up to its next synchronization time
5.	Reconcile the grid with grids with identical rank
6.	Stage boundary data to be provided to higher ranked grids
7.	Apply data from higher ranked grids to complete two-way nesting
8.	Stage data to be provided to lower ranked grids
9.	Perform output if requested

Details of the implementation of the mosaic management algorithm in WW3 can be found in Tolman (2007, Section 3.4) and in Tolman (2008, Section 3.9.2). Note that this implementation required some major modifications to WW3, in particular the introduction of a dynamic data storage for an arbitrary number of grids in a single executable program. Since these modifications to WW3 are of a technical rather than scientific nature, they will not be discussed here (for details see Tolman, 2007, Section 3).

One adaptation of WW3 is introduced particularly for the mosaic approach, and therefore needs to be mentioned here. In previous versions, spatial grid points could be excluded from the computational grid by designating them as land. In the updated model version a distinction between land points and excluded sea points is made. This makes it possible to carve out arbitrary computational domains from a conventional rectangular grid, without introducing spurious land into the model.

3. Two-way nesting

Providing boundary data from lower resolution grids to higher resolution grids has been common practice in wave models for decades. This is relevant for propagation in physical space only. In WW3, the fractional step that addresses spatial propagation solves a reduced version of the general spectral action balance Eq. (1), given as

$$\frac{\partial N}{\partial t} + \nabla_x \cdot \boldsymbol{c}_x N = 0. \tag{3}$$

Several numerical schemes are available. All have been expressed in a flux form, assuring numerical conservation of wave action independent of the actual scheme used. For simplicity considering one dimensional propagation in x-space only, the numerical scheme in flux form becomes

$$N_i^{n+1} = N_i^n + \frac{\Delta t}{\Delta x}[M_{i,i-1} - M_{i,i+1}], \tag{4}$$

where n and i are discrete time and space counters, Δt and Δx are the discrete time and space increments, and $M_{i,i-1}$ represents the action flux through the cell boundary between grids points with counters i and $i-1$. The fluxes are defined as

$$M_{i,i-1} = [c_{x,b} N_b]_{i,i-1}^n, \tag{5}$$

$$c_{x,b} = 0.5(c_{x,i} + c_{x,i-1}), \tag{6}$$

where $c_{x,b}$ is the characteristic velocity at the cell boundary, and N_b is the action density at the cell boundary. The definition of N_b determines the actual scheme. In WW3, a conventional first-order 'upwind' scheme and a third-order ULTIMATE QUICKEST scheme (Leonard, 1979, 1991) are available. Below, these schemes will be denoted simply as the first and third-order schemes. Higher-order schemes are utilized at cell boundaries between sea points only. At cell boundaries sea and land (excluded) points, a first-order (boundary) scheme is employed, assuming zero wave action or energy at the land point.

Boundary data are applied to the model by designating selected grid points as active boundary points. At these grid points, wave conditions are updated directly from the lower resolution grid, rather than dynamically according to Eq. (1). At cell boundaries between active boundary points and regular grid points the first-order boundary scheme is employed, to ensure absorption of outgoing wave action, and to introduce incoming wave action. The wave data from the lower resolution grid are linearly interpolated in space to provide boundary data at the appropriate (higher) spatial resolution. Typically, higher resolution grids are run with smaller time steps. To provide boundary data at each time step, wave data from the lower resolution grid are also linearly interpolated in time.

Several remarks need to be made considering this traditional nesting approach. First, wave action is the conserved quantity in Eq. (1), and therefore should be considered in the data transfer between grids. However, wave energy is the generally preferred diagnostic output of the model, particularly in operational wave modeling. If the mean ocean state (currents and depths) between source and target grids are inconsistent, consistent wave action between grids will result in inconsistent (discontinuous) wave energy between grids. To avoid this, energy rather than action is transferred between grids.

Second, the flux form of Eq. (4) guarantees the conservation of wave action within individual grids. Conservation between grids can only be assured if fluxes are transferred between grids. This, however, may lead to spectral inconsistencies between grids, if inconsistent depths or currents result in input boundary fluxes from the lower ranked grids that are inconsistent fluxes in the interior of the higher ranked grids. In particular for operational wave modeling, it appears preferable to transfer spectral data between grids to assure maximum consistency of solutions between grids. Note that this conservation issue occurs only at the interface between grids. Since such interfaces generally represent a minor part of the entire grid, it is not expected to have a significant impact on model results.

Third, to be consistent with the numerical propagation scheme (4), boundary data are updated at the end of the model time step. In previous versions of WW3, boundary data were erroneously updated at the beginning of the model time step. This spuriously shifted the solution in the high resolution grid forward in time by Δt. In the present version of WW3 this error has been removed.

So far, only conventional one-way nesting has been considered. Two-way nesting is introduced when wave data from the higher resolution grid are introduced back into the lower resolution grids, after the higher resolution grid has caught up in time with the lower resolution grid. The spectral data of grid point i in the low resolution grid ($N_{l,i}$) is computed from spectral data at grids points j in the high resolution grid ($N_{h,j}$) as

$$N_{l,i} = \sum_j w_{i,j} N_{h,j}, \tag{7}$$

where $w_{i,j}$ are weights, defined as the surface of grid cell j in the high resolution grid that covers the grid cell i in the low resolution grid, normalized with the surface of grid cell i. In the degenerate case where resolutions are identical and grids coincide, $N_{l,i} = N_{h,j}$ for the coinciding grid points.

Several remarks need to be made on this two-way nesting approach. First, WW3 considers wave energy rather than action in Eq. (7), consistent with the transfer of boundary data as discussed above.

Second, Eq. (7) is not applied to grid points in the low resolution grid that contribute to boundary data for the high resolution grid. This avoids cyclic updating of data between grids. Such cyclic updating is expected to aggravate conservation issues at grid boundaries as discussed above.

Third, in the area where the low resolution grid is covered by the high resolution grid, low resolution data are updated from the high resolution grid at every model time step of the low resolution grid. Around the edges of the high resolution grid, only a narrow range of grid points contribute dynamically to the low resolution grid solution. The width of this area depends on the number of grid points considered in the numerical scheme (also known as the stencil width). Wave conditions inside the covered area of the low resolution grid therefore do not need to be considered in the low resolution model run, and can therefore be removed from the active computational domain. In the implementation in

WW3, this masking can be done for computation only, or for computation and two-way nesting of Eq. (7), as will be demonstrated below.

The two-way nesting technique can be tested with a simple propagation test with two grids (see Fig. 1). A Cartesian outer grid covers a 1000×1000 km^2 area with a resolution of 25 km. An inner grid covers an area of 300×300 km^2, with the lower left grid point at (600,600) of the outer grid. The water depth in both grids $d = 1000$ m. A test output point is located at the center of the inner grid. Two inner grid resolutions are considered. A degenerate case with $\Delta x = 25$ km as in the outer grid, and a conventional higher resolution grid with $\Delta x = 12.5$ km. In both cases, grid points of the outer grid coincide with grid points of the inner grid in the jointly covered area. The initial conditions consist of monochromatic unidirectional waves with a period of 10 s, traveling at a 45° angle with the grids (Fig. 1b). Time steps are $\Delta t = 15$ min for the 25 km resolution grids and $\Delta t = 7.5$ min for the 12.5 km resolution grid. The waves travel to the output point in approximately 24 h. Computations are performed for 48 h. Propagation test are performed with the first-order and third-order schemes, resulting in a total of four nested cases (two inner grids and two schemes). For reference purposes, wave heights H_s for the outer grid only (no nesting) after 24 h of computation are presented in Fig. 2. The exact solution advects the initial distribution without changing the shape of the spatial wave height distribution. As expected (e.g. Fletcher, 1988), the first-order scheme displays significant numerical diffusion, spreading out the solution in space and lowering the maximum wave height. The third-order scheme advects the wave height distribution without major distortions of its shape. The minor reduction of the maximum wave height and slight 'squaring' of the spatial wave height distribution are well-documented features of the third-order scheme used here.

Model results for the four different mosaic approaches after 24 h are presented in Fig. 3. These figures are constructed by plotting the results of the inner grid directly on top of the results of the outer grid, with exception of panel a, where results of the inner grid are not plotted. Fig. 4 presents the normalized wave height difference ΔH_n at the output point located at the center of the inner grid

$$\Delta H_n = \frac{H_{s,mi} - H_{s,oo}}{H_{s,\max,t=0}}, \tag{8}$$

where $H_{s,mi}$ is the wave height in the inner grid obtained using the mosaic approach, $H_{s,oo}$ is the wave height from the outer grid, obtained by running the outer grid only, and $H_{s,\max,t=0}$ is the maximum wave height in the initial conditions.

Consider first the degenerate case with inner and outer grids with identical resolution and coinciding grid points. The mosaic management algorithm results in a simple alternate computation of both grids. First the outer grid solution is propagated in time by Δt. With the boundary conditions from the outer grid, the inner grid solution then is propagated in time by Δt, after which spectral data from grid points of the inner grid are copied back to the corresponding grid points of the outer grid. For the first-order scheme, the boundary scheme employed between active boundary points and internal grid point in the inner grid is identical to the scheme used throughout both grids. Hence, this degenerate two-way nested case with the first-order scheme should produce results that are identical to results obtained when considering the outer grid only. Indeed, $\Delta H_n \equiv 0$ for this case (solid line in Fig. 4a), as expected, and the composite wave height of both grid is identical to Fig. 2a. Fig. 3a presents the results of the outer grid from the two-way nested approach, to illustrate that the identical composite results can be obtained while foregoing model computations in the masked (gray) area of the outer grid.

When the degenerate case is run with a third-order scheme, differences occur between the nested run and the corresponding single grid run. This can be observed when comparing wave height distributions in Fig. 2b (outer grid model only) with Fig. 3c (nested model). Furthermore, normalized wave height differences at the output point $\Delta H_n \neq 0$ (solid line in Fig. 4b). The differences between the model runs are due to the introduction of an 'internal boundary' in the inner grid where data from the outer grid are provided as boundary data. At this boundary, a local degeneration of the propagation scheme occurs. The internal boundary results in a spatial shift of the wave height distribution, and a reduction of the maximum wave heights.

The test cases where the resolution of the inner grid is higher than the resolution of the outer grids represents a conventional nesting scenario. In this case, the time step of the outer grid Δt_o is twice the time step of the inner grid Δt_i. The mosaic management algorithm will first propagate the solution of the outer grid by Δt_o. Next the solution of the inner grid will be propagated by

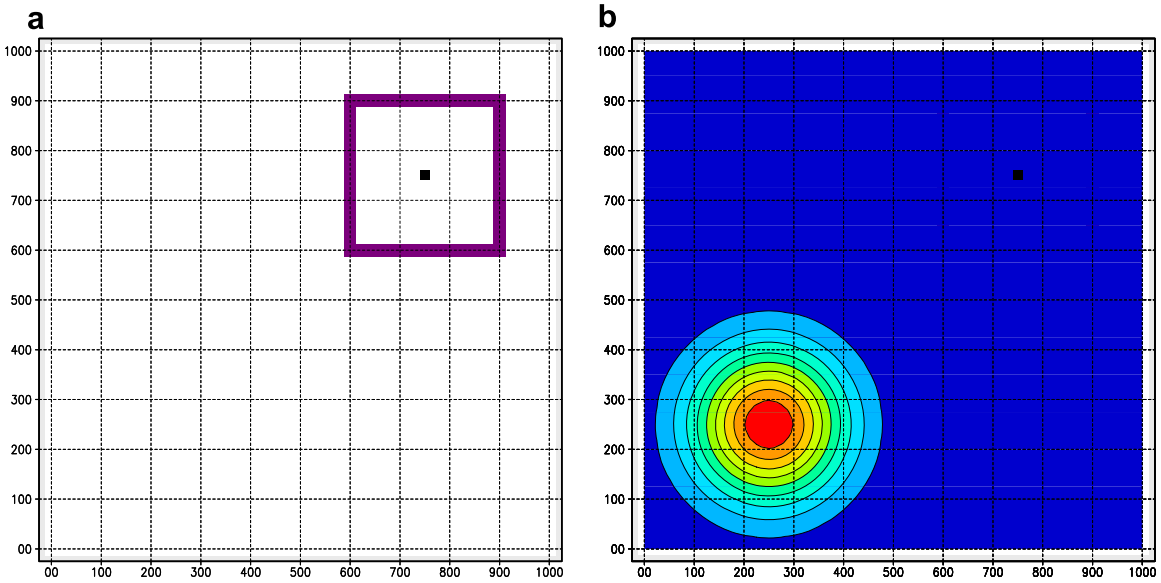

Fig. 1. Test for two way nesting with two grids. (a) Outer grid domain with inner grid superimposed. Boundary grid cells of inner grid are purple. (b) Initial wave heights H_s with contour intervals at $0.1H_{s,\max}$. Monochromatic unidirectional waves with a period $T = 10$ s moving to the upper right corner of the grid. Symbol: output point.

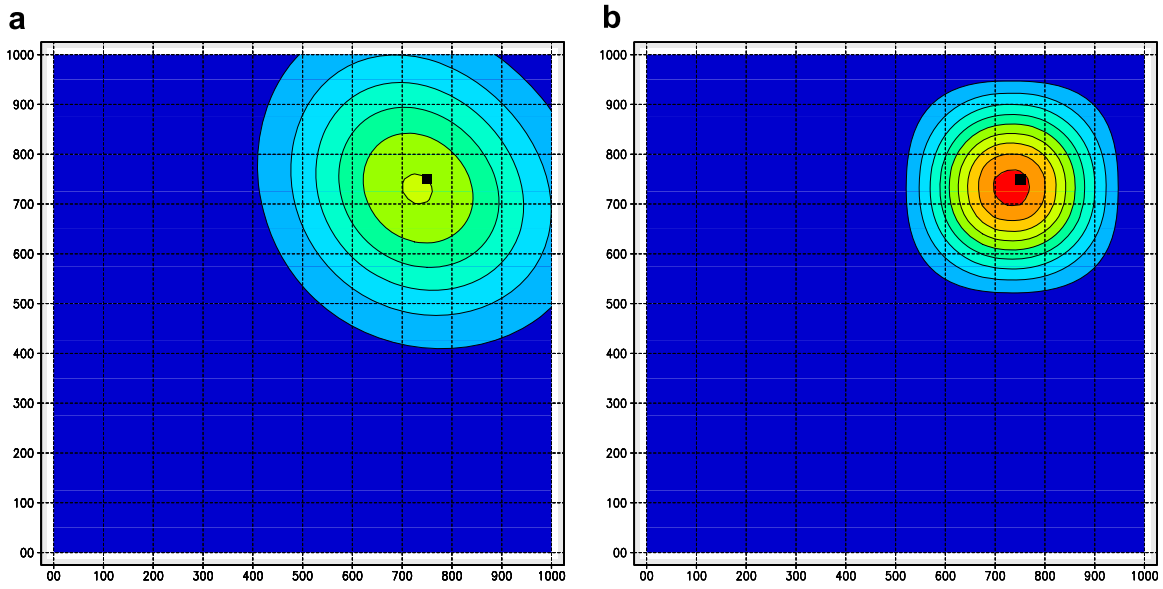

Fig. 2. Wave heights H_s for model runs with outer grid only after 24 h for (a) the first-order scheme and (b) the third-order scheme. Legend as in Fig. 1.

two time steps Δt_i, using boundary data from the outer grid, interpolated in space and time for each individual time step Δt_i. Finally, results of the inner grid are converted to the appropriate grid points of the outer grid by spatial averaging, and the mosaic results for the next time are obtained.

For the first-order scheme, the increased resolution of the inner grid will reduce numerical diffusion (e.g. Fletcher, 1988). Fig. 4a (dashed line) shows the three-lobed structure of the wave height differences ΔH_n, indicating a higher maximum wave height and a wave height distribution that is narrower. Both features are indicative of reduced numerical diffusion. Although the differences are small, this can also be observed when comparing spatial wave height distributions in Fig. 2 and 3a and b (mostly near the maximum wave height).

For the third-order scheme, increased resolution has a much smaller impact on numerical diffusion (e.g. Fletcher, 1988). However, the increased resolution reduces the impact of the degenerated scheme at the internal boundary in the inner grid. Hence, differences between this nested case and the outer-grid-only case in fact become smaller than for the degenerate case. This is particularly clear when comparing the solid and dashed lines in Fig. 4b.

The test considered above is designed to demonstrate the capability of the nesting techniques, but does not represent a case for which nesting is particularly beneficial, nor does it demonstrate nesting in a full wave model with active wave generation. A second test illustrates the practical capabilities of the nesting approach. Wave growth in hurricane conditions is considered using a set of three telescoping nests, all centered on the eye of the hurricane. All grids are square with sizes of 2500, 750 and 250 km, and grid increments Δx of 50, 15 and 5 km, respectively. Note that the grid increments are not integer multiples. The wind field is described as a Rankin vortex with a radius of maximum wind of 50 km, and with a maximum wind speed of 45 ms^{-1}. A conventional spectral grid with 24 directions and 25 frequencies and the default model setting of WW3 are used. Time steps of the three grids are 1800, 600 and 200 s. The water depth is 1000 m in all grids. Additionally, the moving grid option of Tolman and Alves (2005) is used, with all grids moving to the right with a speed of 5 ms^{-1}.

The mosaic management algorithm will first propagate the solution of the first grid by 1800 s. This provides the boundary conditions for propagating the solution for the second grid by 600 s. This in turn provides boundary conditions to propagate the solution of the third grid by three steps of 200 s to catch up with the second grid. Data from the third grid then are averaged back into the second grid. This interplay between the second and third grid continues until the solutions for all grids are propagated by 1800 s, after which the data of the second grid are averaged back into the first grid, completing on 1800 s time step of the entire mosaic approach.

Fig. 5 shows wave heights from the three individual grids obtained with the two-way nesting approach (panels a through c). Note that the figure only covers part of the outer domain, and that the option to mask out part of the computational domain of lower resolution grids has been used (gray shading in panels a and b). Fig. 5d shows the composite of the results for the three grids. Clearly, the three grids represent a consistent mosaic with resolution increasing by an order of magnitude from the outside of the figure to the inside of the figure. Some minor inconsistencies appear to exist in the upper right corner of the central grid (Fig. 5b). Such discrepancies appear to occur mainly in corners of grids when lines of boundary points line up with grid axes, and appear to be related to different scales of spatial smoothing employed in the grids to avoid the so-called garden sprinkler effect (see, e.g. Booij and Holthuijsen, 1987; Tolman, 2002). They become rare or non-existent when more irregular computational domains are carved out from nested grids (figures not presented here).

The main wave generation area is contained in the inner grid. Conversely, wave conditions in the outer grid are swell dominated. The masked out area in the outer grid (gray area in Fig. 5a) clearly indicates that these swells are generated in the inner grid and passed on to the outer grid using the two-way nesting approach. Note, furthermore, that the outer grid does not resolve the wind field, because the grid increment and the radius of maximum wind both are 50 km. Hence, consistent results between all grids can only be obtained using a two-way nesting approach.

Results of additional tests of the two-way nesting approach, including propagation over variable depths and currents, and additional hurricane tests using circular computational domains can be found in Tolman (2006), (2007).

4. Overlapping grids

In Section 1, reasons for allowing grids with similar or identical resolutions to overlap are presented. In such a case, no clear order

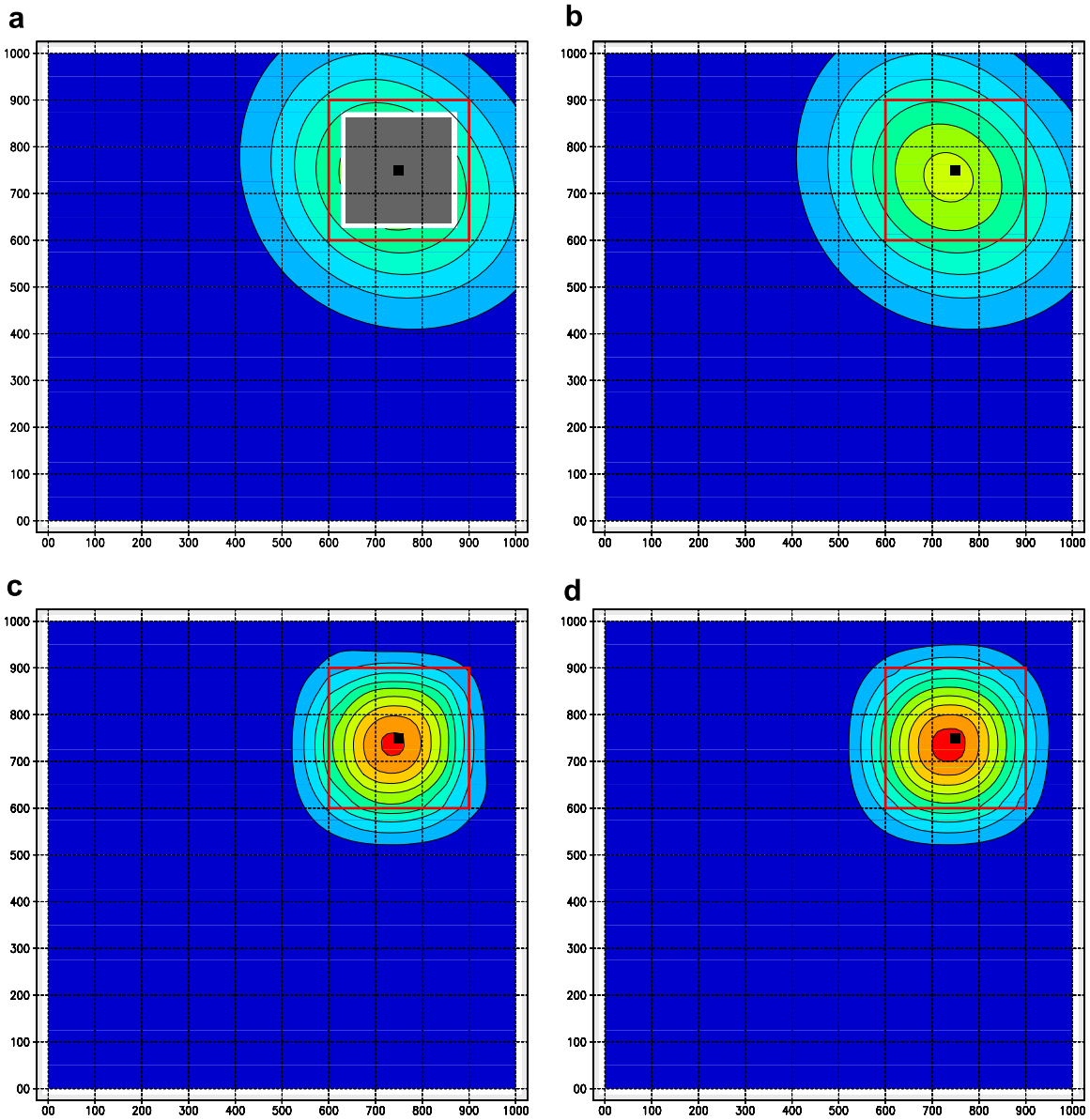

Fig. 3. Wave heights H_s for two-way coupled model runs after 24 h. Results of inner grid plotted on top of results for outer grid. Red box identifies the location of input boundary grid points of the inner grid. (left panels) 25 km resolution inner grid. (right panels) 12.5 km resolution inner grid. (top panels) First-order scheme. (bottom panels) Third-order scheme. In panel (a) only the outer grid results are plotted, and the gray shading identifies grid cells removed from the computation. The white band around the shaded area occurs because the wave height contouring extends only to the center of the cells next to the masked cells.

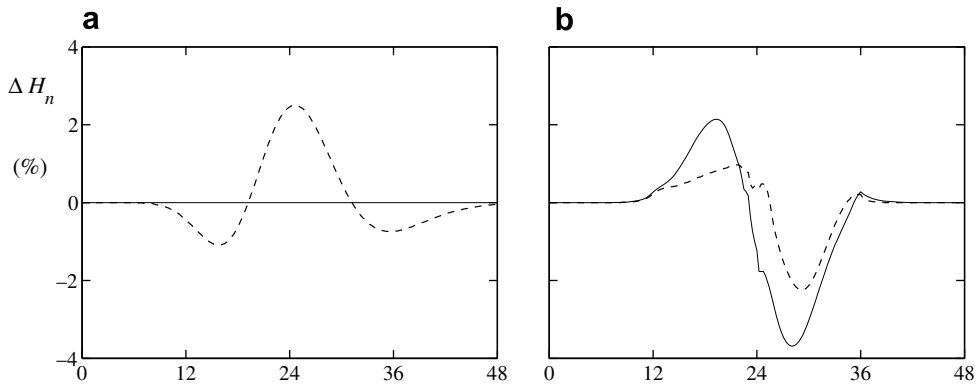

Fig. 4. Wave heights differences between inner grid in two-way nested approach and outer grid only run, normalized with the maximum wave height in the initial conditions (ΔH_n) corresponding to test results presented in Fig. 3. (a) First-order scheme. (b) Third-order scheme. (solid lines) 25 km inner grid resolution. (dashed lines) 12.5 km inner grid resolution.

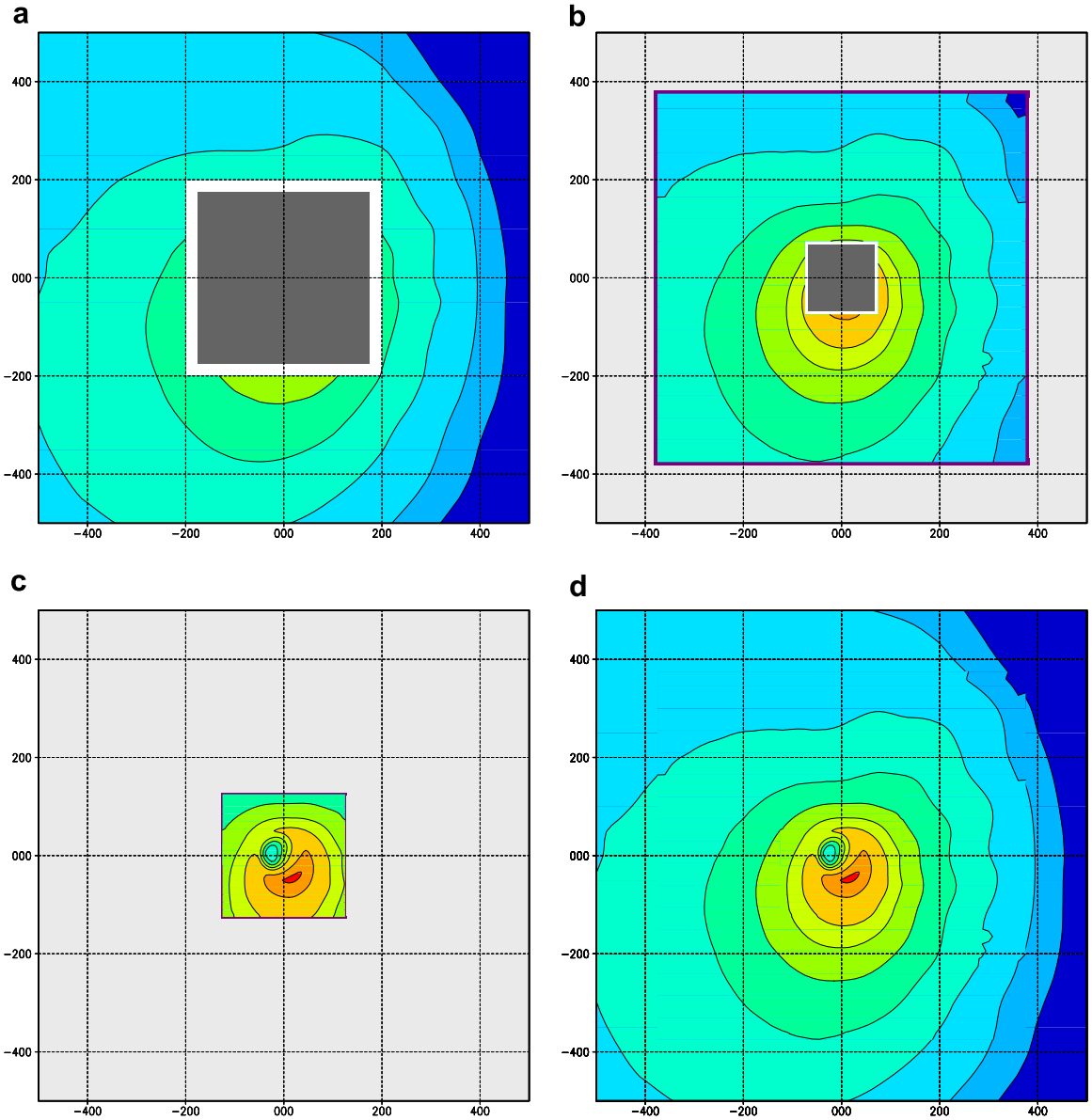

Fig. 5. Wave heights H_s from the moving grid hurricane wave generation test for the three grids making up the mosaic (a–c) and the composite mosaic results (d). Wave heights at 1 m intervals. $H_{s,\max} > 10$ m. Masked grid cells are shaded gray. Input boundary grid cells are shaded purple. White space between gray shading and wave height data is an artifact of plotting techniques used (see also Fig. 3).

of computation can be established. Instead, the solution for all overlapping grids is propagated by a common time step Δt, after which the grids are reconciled to produce the proper unified solution.

Breaking up a grid in several overlapping grids introduces artificial internal boundaries. From these boundaries, errors propagate into the grid. The distance over which such errors propagate in a time step Δt depends on the stencil width of the numerical scheme. Inside this area, results in the grid need to be replaced by results from overlapping grids that are not impacted by their own spurious results near boundaries. This implies that grids need to overlap sufficiently to assure that areas where effects of artificial boundaries intrude into grids do not overlap. This may leave a part of the overlap between grids where neither of the grids are influenced by the artificial boundaries. If the grids and forcing are consistent, results in these areas could be left unchanged. However, to

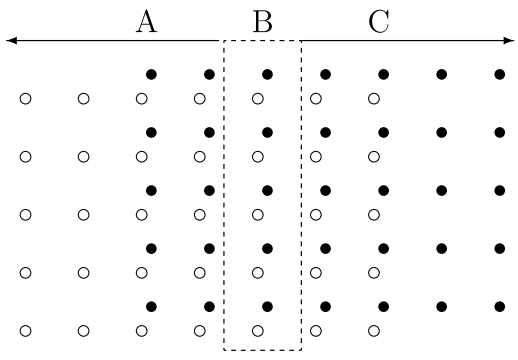

Fig. 6. Concept for reconciling grids with similar resolution. (○) Points of grid 1 and (●) grid 2. Errors from artificial internal boundaries propagate by two grid points per time step.

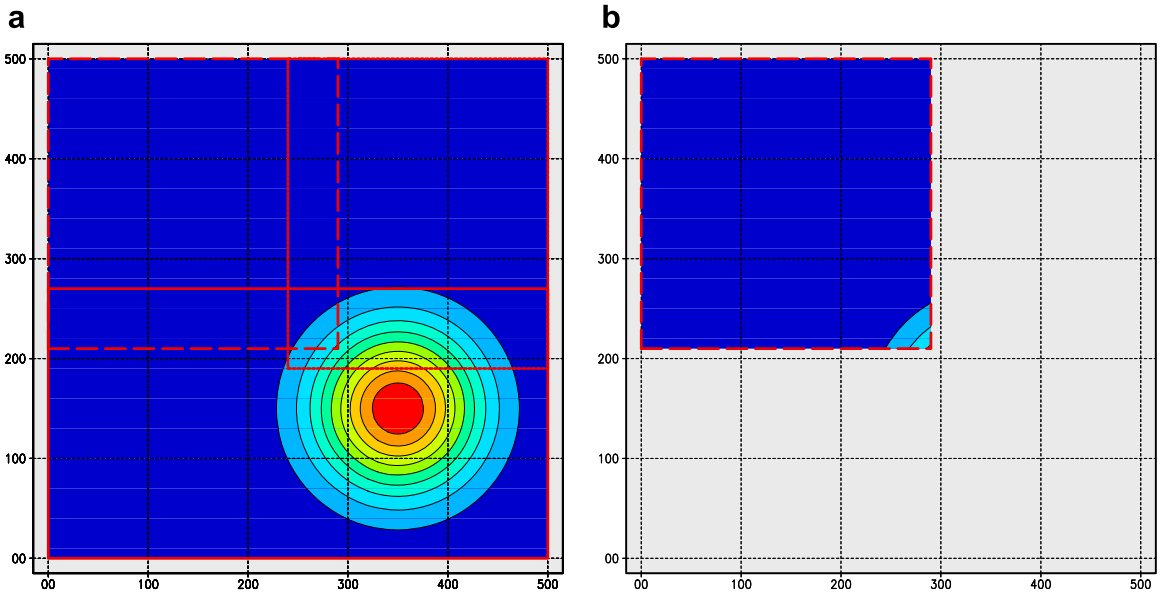

Fig. 7. Initial conditions for test of overlapping grids. The red boxes identify the three grids extracted from the master grid. (a) Single grid or composite of grids. (b) Upper left grid only. Contour lines at 10% increments of the maximum wave height.

add robustness to the reconciliation, linear interpolation of spectra from all grids considered is applied to such areas in WW3. The interpolation weights are set as proportional to the distance to the areas influenced by the artificial boundaries in each individual grid.

Fig. 6 illustrates the concept of grid reconciliation. Two grids with similar resolution but with a shift in grid points overlap. An area of two grid points is influenced by the artificial internal boundaries. Grid 1 (○ in Fig. 6) thus has spurious boundary intrusion in the area identified by 'C', but has valid results in areas A and B. Similarly, grid 2 (●) has spurious boundary intrusion in area A, and valid results in areas B and C. In the contaminated areas (area C for grid 1 and area A for grid 2) results are replaced by valid results from the other grid. Because the grids do not coincide, the replacements are obtained by linear interpolation in space from the source grid. In the central overlap area B results are obtained as the average of both grids, again interpolating as necessary. Note that data transfer between grids is performed using wave energy instead of action, consistent with the approach used for nesting as described in Section 3.

The reconciliation technique can be demonstrated with the simple swell propagation test. Consider an area with a constant depth of $d = 250$m and with a resolution of $\Delta x = 10$ km. Swell propagation in this area is considered using a single grid, or three individual overlapping grids. Fig. 7 shows the initial conditions for this test and the layout of the three grids. Monochromatic swells with a wave period of 10 s traveling to the upper left corner of the grid are considered. Note that this setup of grids was made to illustrate the proper workings of the reconciliation methods introduced here. For such small grids, it is obviously not practical to subdivide the grid in even smaller pieces.

With the three grids taken from a single master grid, all resolutions are identical and all grid points in grid overlaps coincide. If the overlap areas are wide enough, this should produce identical results for the single grid and for the mosaic of the three separate grids. Fig. 8 shows the results of 6 h of model integration with the third-order scheme. Indeed, results of the two approaches are identical. Note that the upper left grid obtains its 'boundary data' from the reconciliation techniques, as is clear from a comparison of Figs. 7 and 8b.

To illustrate the interaction between this reconciliation technique with the two-way nesting, three higher-resolution grids ($\Delta x = 5$ km) have been added to this test. A curved (circular) coastline is introduced with a beach with a constant shore-normal slope. The mosaic management algorithm will first propagate the solution of the three low resolution grids of Fig. 7 (red boxes) over their time step Δt. After grid results are reconciled, boundary data are posted to the three high resolution grids shown in Fig. 9. The solution for the latter grids is then propagated over $0.5\Delta t$, and the results of these three grids are reconciled. This procedure is repeated to propagate the solution of the high resolution grids over a total of Δt. Averaging the results from the high resolution grids back into the low resolution grids completes the time step Δt.

Fig. 10 shows model results for a composite of the six grids after 6 and 12 h of model integration. The swell field consistently propagates through all six grids, and shoals on the coastline. As expected, the results are identical to those of a nested model runs with a single low resolution grid, and/or a single high resolution grid (figures not presented here). Note that if the overlapping grids are not completely consistent (small differences in resolution or shifted grids) similar consistent results are found between grids (figures not presented here). However, such results are no longer identical to those obtained with a single low and high resolution grid, due to minor differences introduced by interpolation between grids (for examples, see Tolman, 2007).

5. An application to Alaskan waters

After the idealized test cases presented above, the mosaic approach will now be applied to a hindcast for Alaskan coastal waters. A system of three grids, telescoping in on the Alaskan coast has been developed using the ETOPO2 bathymetry data[1] and the Global Self contained Hierarchical High resolution Shoreline data (GSHHS, Wessel and Smith, 1996), using the grid generation tools developed by Chawla and Tolman (2007), Chawla and Tolman (2008). The layout of these grids is illustrated in Fig. 11. The first grid in this model is a 1° resolution Pacific basin grid (Fig. 11a). This grid extends far enough north only to transition to the second grid, and the northern most part of the grid is masked out of the computations. The second grid is a conventional regional grid with a resolu-

[1] http://www.ngdg.noaa.gov/mgg/fliers/01mgg04.html.

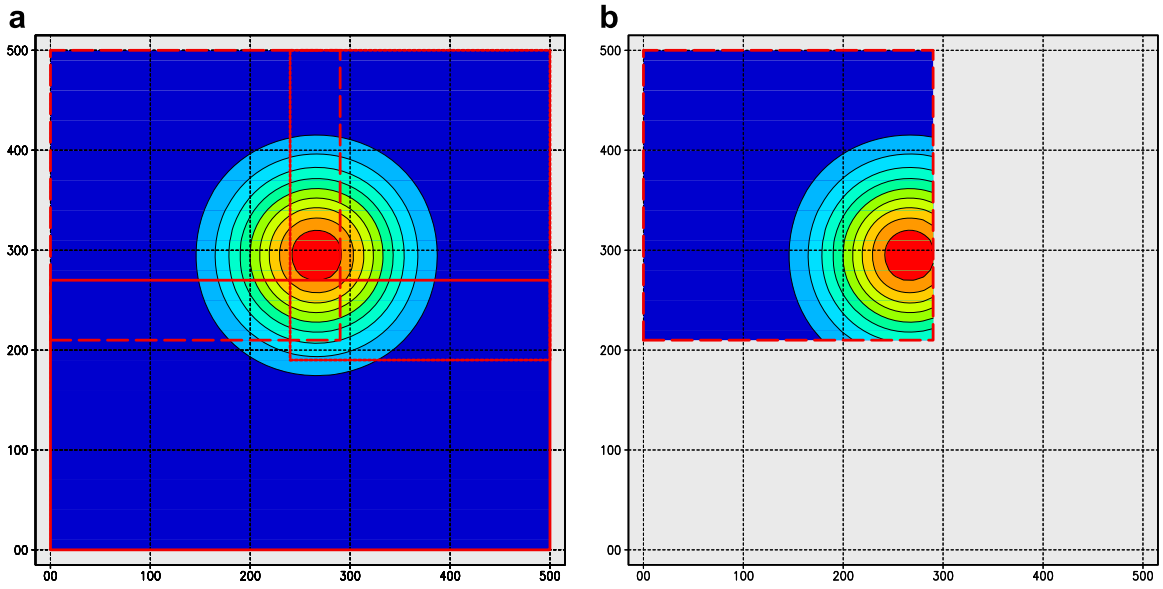

Fig. 8. Swell propagation after 6 h with the third-order scheme for the initial conditions and grid of Fig. 7. (a) Results for a single grid or composite of three grids. (b) Results for the upper left grid only. Legend as in Fig. 7.

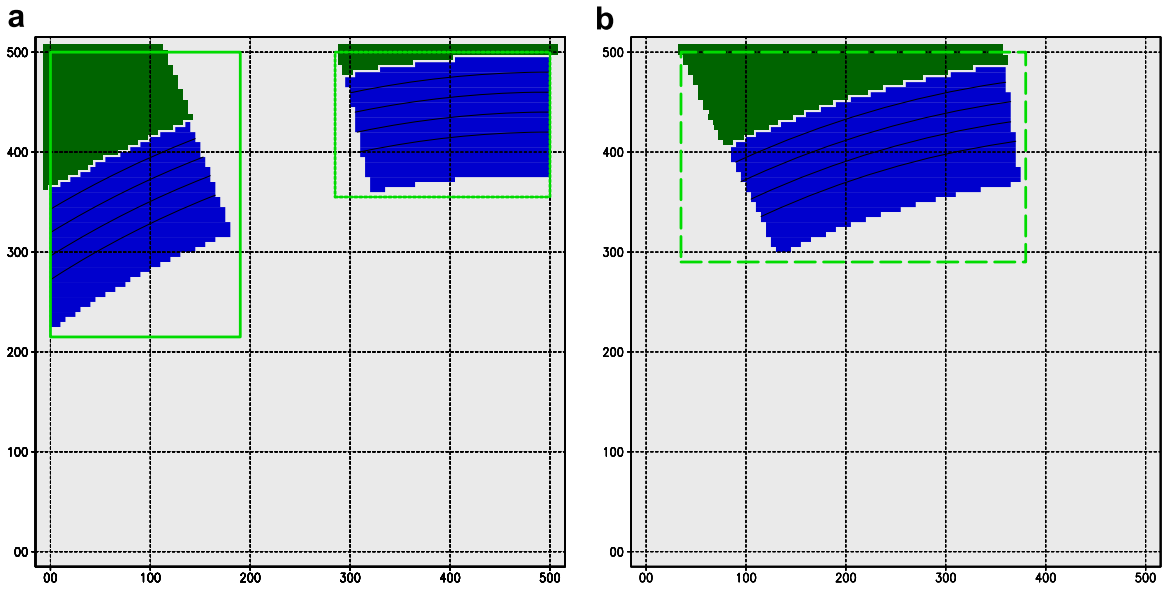

Fig. 9. Layout of high-resolution grids for test added to the swell propagation test illustrated in Fig. 7. Solid lines in blue-shaded areas identify depth contours at 50 m intervals Green shaded areas identify land. (a) Outside grids. (b) Central grid. The green boxes identify the extend of the individual grids. Note that the computational domains (blue shaded areas) are a subset of the grid extend.

tion of $^1/_2^\circ \times {}^1/_4^\circ$ (Fig. 11b). It receives boundary data in the southern half of the grid only. The third and final grid is a 'coastal' grid with a resolution of $^1/_8^\circ \times {}^1/_{16}^\circ$ (Fig. 11c). The coastal grid covers an area similar to that of the regional grid. However, the coastal grid is defined as a sparse grid using near-coastal grid points only.

Normally, WW3 grids consist of bathymetric information, a land–sea mask, and obstruction grids to represent islands that are not resolved by the grid (Tolman, 2003). To illustrate the capability of the mosaic approach to represent islands by means of locally increasing the model resolution, obstruction grids have not been used in WW3 in this test case.

Wind and ice data for this application for January 2006 have been taken from NCEP's operational model suite. Winds are provided on a 1° spatial resolution and a 3 h time resolution from NCEP's Global Forecast System (GFS, Environmental Modeling Center, 2003), Ice fields are obtained from NCEP's 5′ global ice concentration analysis (conform to Grumbine, 1996), and are updated every 3 days. In the mosaic version of WW3 these input data fields are interpolated or averaged to individual grids internally in the model, to assure maximum consistency of forcing between individual grids. The model starts from calm conditions on January 1, 2006, 0000 UTC.

The mosaic approach gives consistent results for all grids for the entire month of January 2006. An example of this consistency is given in Fig. 12 for the northern Pacific Ocean valid for January 16, 2006, 0000 UTC. Note that the transition between grids in this figure is obvious in the change of resolution of the land–sea mask only.

Of particular interest is the capability of the mosaic approach to explicitly block the propagation of swell by islands. This is

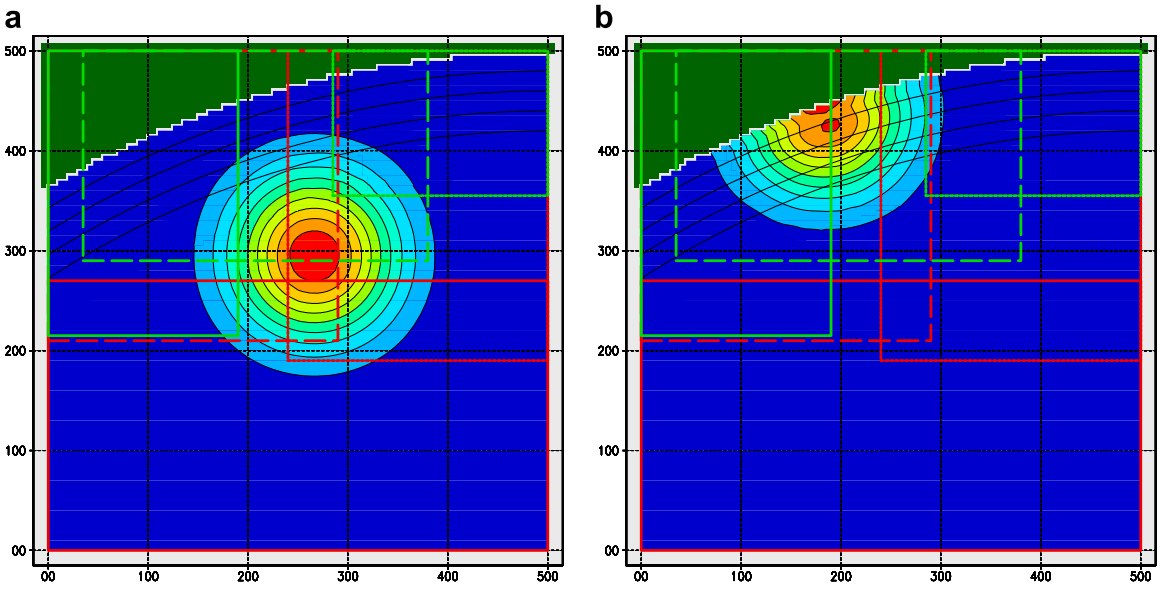

Fig. 10. Swell propagation with the third-order scheme for the test case with the six grids identified in Figs. 7 and 9 after (a) 6 h and (b) 12 h of model integration. Legend as in Fig. 7.

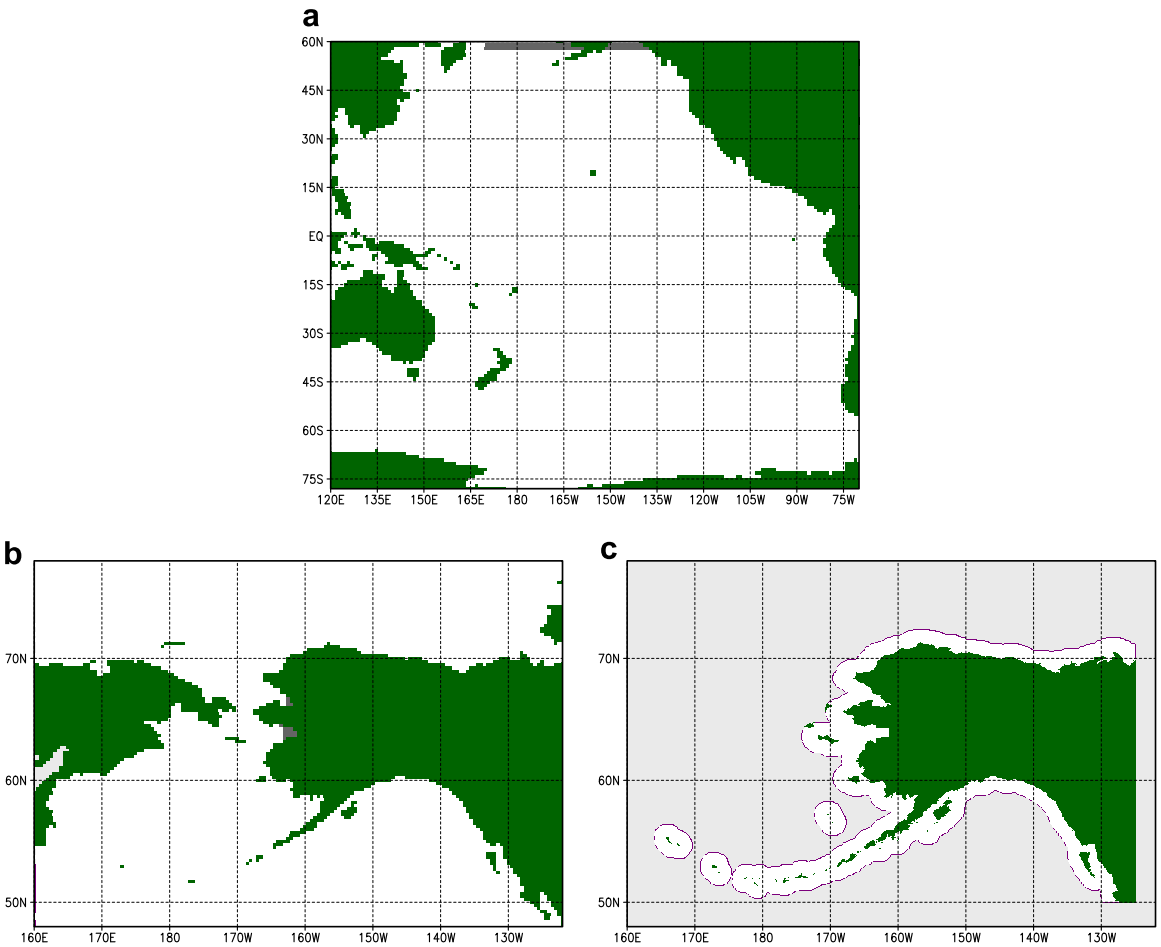

Fig. 11. Wave grids for the Alaskan. (a) Basin grid with 1° resolution. (b) Regional grid (1/2° × 1/4°). (c) Coastal grid (1/8° × 1/16°). Light gray identifies areas not considered in the grid. Dark gray identifies areas masked out in the computation. Purple identifies active boundary points.

illustrated for part of the Aleutian islands in Fig. 13, displaying results for the coastal and regional grids only. The coastal grid explicitly resolves many of the Aleutian islands, and result in clear shadow zones around the islands. Note that unresolved islands are not included as obstructions, as discussed above. In Fig. 13a, such shadow zones occur to the south of the resolved islands. In

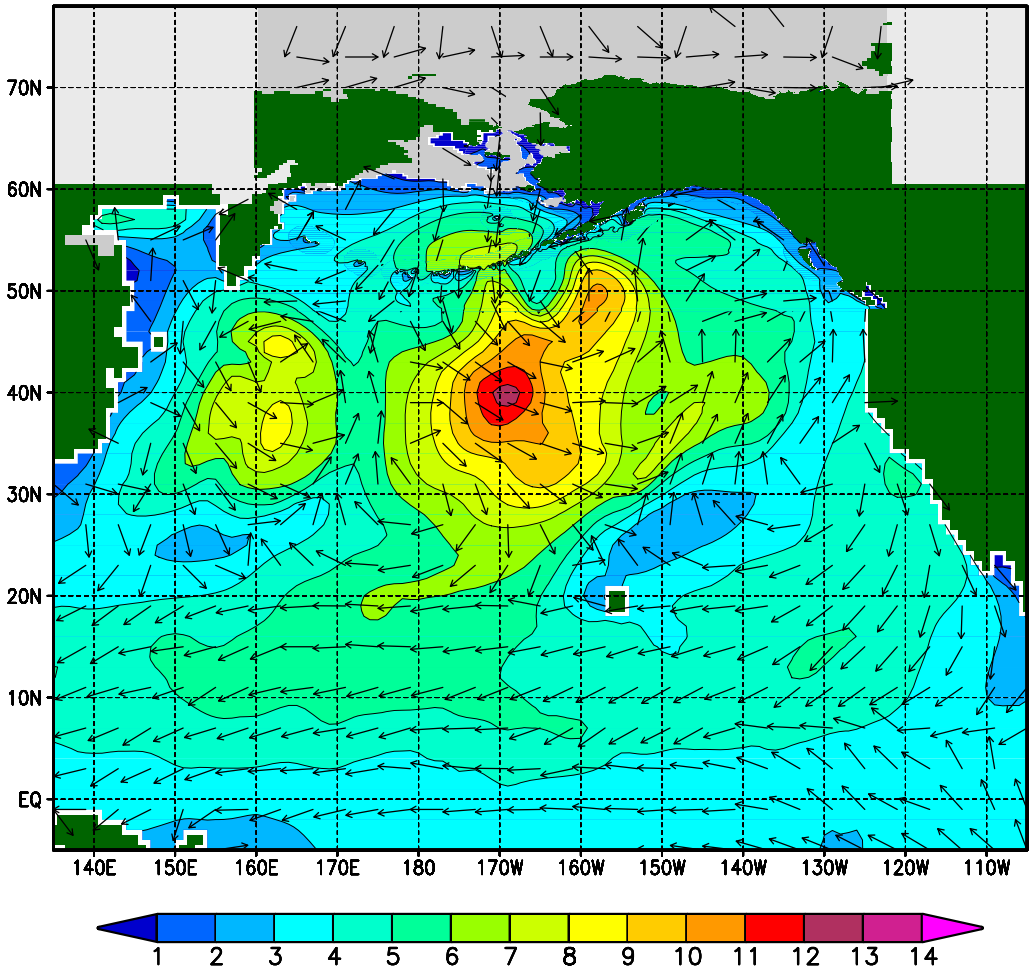

Fig. 12. Wave heights H_s in meters for the North Pacific Ocean from the Alaskan waters test case for Jan 16, 2006, 00 UTC. Vectors identify peak wave direction.

the regional grid (Fig. 13b) only a few of the islands are partially resolved. Nevertheless, the shadow effect of the islands that are resolved in the coastal grid are clearly visible in this regional grid. Because these islands are not described as sub-grid obstacles, the blocking is clearly due to the two-way nesting employed in the mosaic approach.

6. Discussion

This study presents a mosaic or multi-grid approach to wind wave modeling. In this approach, an area of interest is covered with an arbitrary number of grids with resolutions as required locally. All grids are considered as individual wave models. However, by considering continuous data exchange between such grids/models, the mosaic effectively becomes a single wave model. Three types of data exchange between grids are considered. Data from lower resolution grids are provided to higher resolution grids as boundary data. Data from higher resolution grids are averaged back into grid points of lower resolution grids. Overlapping grids with similar resolution are reconciled, removing the influence of artificial internal model boundaries. An algorithm is presented for running all grids concurrently, and for exchanging data between these grids. Both idealized and realistic test cases are presented. The mosaic approach is now being used for operational forecasting at NCEP considering systematic resolution increases from high-seas to offshore and to coastal areas with resolutions of approximately 56, 18 and 7.5 km, respectively (Tolman, 2007; Chawla et al., 2007).

It should be noted that nesting techniques presented here are fundamentally different from nesting techniques presented in circulation modeling for oceans and atmospheres (e.g. Kurihara et al., 1995). In the latter case, the advection velocity of the medium is a part of the solution. Changes or incompatibilities of advection across nesting boundaries then can lead to spurious internal reflections (e.g. Fletcher, 1988), and generally require a 'sponge layer' to damp such oscillations, and/or a weighted average between low and high resolution solutions when feeding the high resolution results back into the low resolution grid. In the spectral balance Eq. (1), however, the characteristic velocity is (at first order) independent of the solution. Therefore, nesting in wave models by definition is not sensitive to spurious internal reflections, and the high resolution model results can fully replace low resolution results in overlap areas. This makes nesting in wave models relatively straightforward.

The present study only deals with a mosaic comprised of static grids. In the introduction, however, hurricane modeling with relocatable grids cf. Kurihara et al. (1995) was identified as a major application area for a mosaic approach. The mosaic approach presented here in principle can be applied to relocatable grids without major modifications. The main issue is the continuous need for remapping of interactions between grids. This is mostly a technical rather than scientific issue. New issues occur only at the edges of high resolution grids that are relocated; in such areas, wave data in a high resolution grid may have to be initialized from a lower resolution grid. This also represents a fairly straightforward

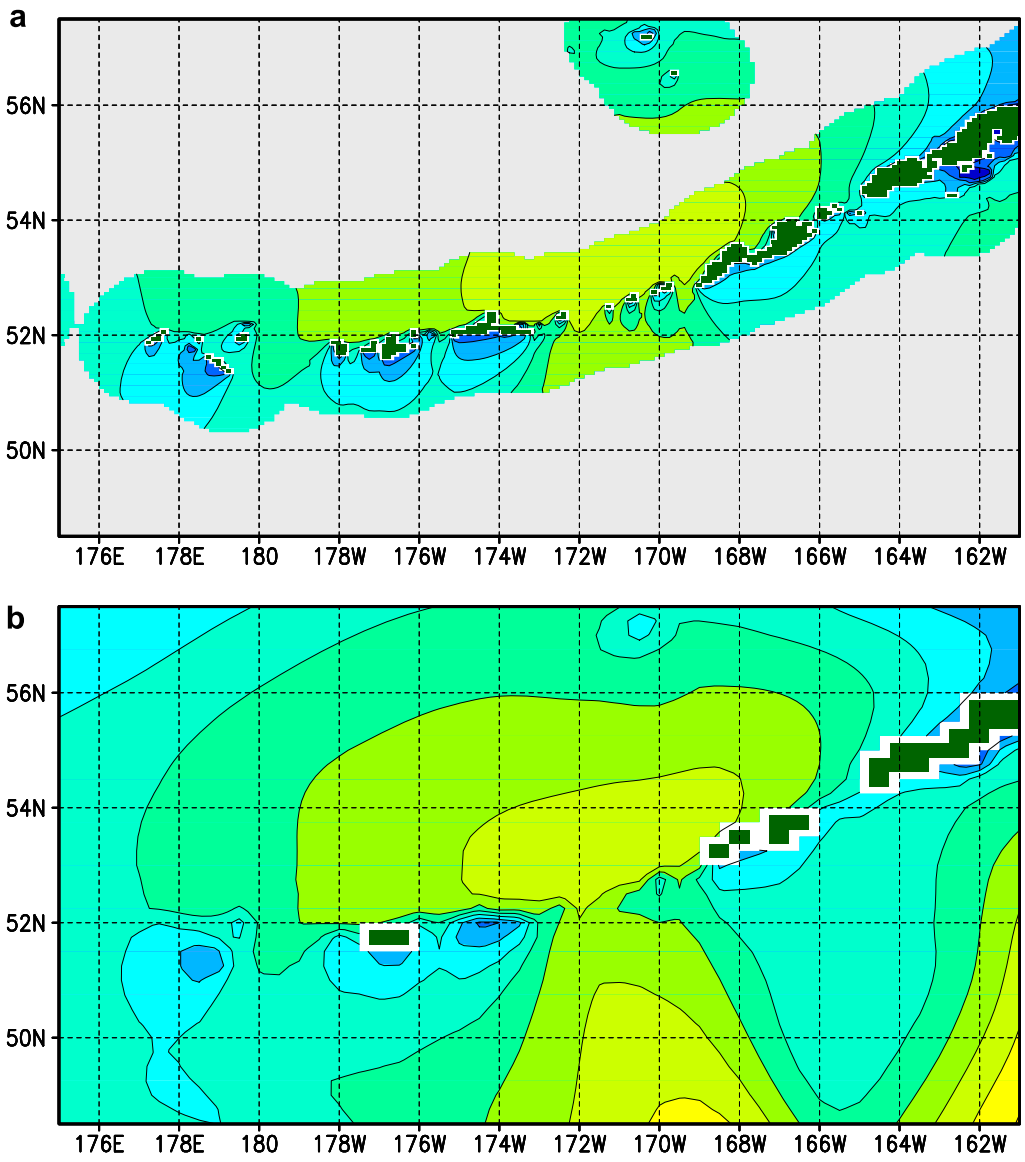

Fig. 13. Detailed model results (H_s) for part of the Aleutian Islands corresponding to Fig. 12. (a) The coastal grid only and (b) the regional grid only.

technical issue. Development of a relocatable mosaic approach is planned at NCEP for integration in hurricane models.

The present approach can be loosely interpreted as a generalization of the stepwise increased resolution introduced by Gomez and Carretero (1997, henceforth denoted as GC97). However, there are two distinct differences. First, GC97 requires integer multiples of grid resolution between areas of different resolution. The present approach uses general interpolation and averaging techniques, and has been implemented in WW3 without limitations on ratios of model resolutions or requirements of coinciding grid points. The present approach is thus more flexible with respect to the layout of the mosaic of grids. Second, the method of GC97 considers a single grid with stepwise increased resolution. The present approach sets up each element of the mosaic as an individual wave grid. The latter allows a 'plug and play' approach to mosaic modeling, where individual grids can be moved in and out of the mosaic with minimal effort. For WW3 the ease of setting up grids is furthermore increased by the grid generation software developed by Chawla and Tolman (2007), (2008).

The mosaic approach adds flexibility to wave modeling by allowing resolution to be focused on selected areas. It is, however, not as flexible as an unstructured grid approach. The advantage of the mosaic approach is the relative ease of grid generation, and the long experience with higher-order numerical schemes to accurately propagate swells. Also, low resolution grids can be run with larger and hence more economical time steps, whereas a single unstructured grid typically requires times steps dictated by the smallest grid meshes. The advantage of the unstructured grid approach is the flexibility to accurately depict dominant bathymetric features. The latter becomes particularly important if inundation and drying out of areas is considered. In this context unstructured grids appear potentially beneficial in coupled wave-surge models. Another application of unstructured grids would be high-latitude wave modeling, in particular wave conditions in Arctic waters in the summer. Typical structured grids become prohibitively expensive in polar waters due to the grid singularity at the North Pole.

Considering the above, the unstructured grid approach of Hsu et al. (2005) is considered for incorporation in WW3. Ideally, this approach can be used side-by-side with structured grids in a mosaic approach, so that benefits of both approaches can be utilized locally. The nesting and reconciliation techniques discussed here can be applied directly to unstructured grids, or to a mosaic

containing both structured and unstructured grids, because of the use of general interpolation and averaging techniques.

7. Conclusions

A mosaic approach to wind wave modeling is presented, where a set of wave model grids is converted into a single wave model by considering two-way interactions between grids. The approach is implemented in the WAVEWATCH III wind wave model. Using this model, the approach is shown to produce consistent results between grids in various idealized wave propagation tests, in an idealized hurricane test, and in a practical application to Alaskan waters. The method provides an effective way to provide targeted (high) resolution to areas of interest. One such application is to explicitly resolve island chains by applying high model resolution only to relevant areas. The consistency of model results between grids is particularly useful for operational wave forecast problems where consistent forecasts at different resolutions are required.

Presently, only static grids are considered in the WAVEWATCH III implementation. For hurricane applications, development of relocatable grids within the mosaic approach appears desirable. The mosaic approach represents an alternative to unstructured grid approaches. Nevertheless, unstructured grids may still be more effective for near-shore and wave-surge applications. The extension of the mosaic approach to relocatable grids, and to a mixture of structured and unstructured grids appears to be relatively straightforward.

Acknowledgements

The author thank D.B. Rao for his support for developing this methodology and the massive software engineering effort it required for the past several years. The author thank Arun Chawla, Todd Spindler, Ken Campana, Young Kwon and the anonymous reviewers for their constructive comments on early drafts of this manuscript.

References

Ardhuin, F., Herbers, T.H.C., O'Reilly, W.C., 2001. A hybrid Eulerian–Lagrangian model for spectral wave evolution with application to bottom friction on the continental shelf. J. Phys. Oceanogr. 31, 1498–1516.

Benoit, M., Marcos, F., Becq, F., 1996. Development of a third generation shallow-water wave model with unstructured spatial meshing. In: Proc. 25th Int. Conf. Coastal Eng., pp. 465–478. ASCE.

Booij, N., Holthuijsen, L.H., 1987. Propagation of ocean waves in discrete spectral wave models. J. Comput. Phys. 68, 307–326.

Booij, N., Ris, R.C., Holthuijsen, L.H., 1999. A third-generation wave model for coastal regions, Part I, model description and validation. J. Geophys. Res. 104, 7649–7666.

Chawla, A., Cao, D., Gerald, V.M., Spindler, T., Tolman, H.L., 2007. Operational implementation of a multi-grid wave forecast system. In: 10th International Workshop on Wave hindcasting and Forecasting & Coastal Hazerd Symposium Paper B3.

Chawla, A., Tolman, H.L., 2007 Automated grid generation for WAVEWATCH III. Tech. Note 254, NOAA/NWS/NCEP/MMAB, 71 pp.

Chawla, A., Tolman, H.L., 2008. Obstruction grids for spectral wave models. Ocean Mod. 22, 12–25.

Environmental Modeling Center. 2003. The GFS atmospheric model. NCEP Office Note 442, NOAA/NWS/NCEP, 14 pp.

Fletcher, C.A.J., 1988. Computational techniques for fluid dynamics, part I and II. Springer, Berlin. 409 + 484 pp.

Gomez, M., Carretero, J.C., 1997. A two-way nesting procedure for the WAM model: application to the Spanish coast. J. Offshore Mech. Arctic Eng. 119, 20–24.

Grumbine, R.W., 1996. Automated passive microwave sea ice concentration analysis at NCEP. Tech. Note 120, NOAA/NWS/NCEP/OMB, 13 pp.

Hsu, T.-W., Ou, S.-H., Liau, J.-M., 2005. Hindcasting near shore wind waves using a FEM code for SWAN. Coastal Eng. 52, 177–195.

Komen, G.J., Cavaleri, L., Donelan, M., Hasselmann, K., Hasselmann, S., Janssen, P.E.A.M., 1994. Dynamics and Modelling of Ocean Waves. Cambridge University Press, Cambridge. 532 pp.

Kurihara, Y., Bender, M.A., Tuleya, R.E., Ross, R.J., 1995. Improvements in the GFDL hurricane prediction system. Mon. Weather Rev. 123, 2791–2801.

Leonard, B.P., 1979. A stable and accurate convective modelling procedure based on quadratic upstream interpolation. Comput. Meth. Appl. Mech. Eng. 18, 59–98.

Leonard, B.P., 1991. The ULTIMATE conservative difference scheme applied to unsteady one-dimensional advection. Comput. Meth. Appl. Mech. Eng. 88, 17–74.

Ris, R.C., Holthuijsen, L.H., Booij, N., 1999. A third-generation wave model for coastal regions, Part II: verification. J. Geophys. Res. 104, 7667–7681.

Tolman, H.L., 1991. A third-generation model for wind waves on slowly varying, unsteady and inhomogeneous depths and currents. J. Phys. Oceanogr. 21, 782–797.

Tolman, H.L., 2002. Alleviating the garden sprinkler effect in wind wave models. Ocean Mod. 4, 269–289.

Tolman, H.L., 2002. User manual and system documentation of WAVEWATCH III version 2.22. Tech. Note 222, NOAA/NWS/NCEP/MMAB,133 pp.

Tolman, H.L., 2003. Treatment of unresolved islands and ice in wind wave models. Ocean Mod. 5, 219–231.

Tolman, H.L., 2006. Toward a third release of WAVEWATCH III; a multi-grid model version. In: Proc. of the 9th International Workshop on Wave Hindcasting and Forecasting, JCOMM Tech. Rep. 34, Paper L1.

Tolman, H.L., 2007. Development of a multi-grid version of WAVEWATCH III. Tech. Note 256, NOAA/NWS/NCEP/MMAB, 88 pp. + Appendices.

Tolman, H.L., 2008. User manual and system documentation of WAVEWATCH III version 3.14. Tech. note 268, NOAA/NWS/NCEP/MMAB, 192 pp.

Tolman, H.L., Alves, J.H.G.M., 2005. Numerical modeling of wind waves generated by tropical cyclones using moving grids. Ocean Mod. 9, 305–323.

Tolman, H.L., Balasubramaniyan, B., Burroughs, L.D., Chalikov, D.V., Chao, Y.Y., Chen, H.S., Gerald, V.M., 2002. Development and implementation of wind generated ocean surface wave models at NCEP. Weather Forecasting 17, 311–333.

Wessel, P., Smith, W., 1996. A global self-consistent hierarchical high resolution shoreline database. J. Geophys. Res. 101, 8741–8743.

Yanenko, N.N., 1971. The Method of Fractional Steps. Springer, Berlin.